

Novel Strongly Correlated Europium Superhydrides

Dmitrii V. Semenok, Di Zhou, Alexander G. Kvashnin, Xiaoli Huang,* Michele Galasso, Ivan A. Kruglov, Anna G. Ivanova, Alexander G. Gavriliuk, Wuhan Chen, Nikolay V. Tkachenko, Alexander I. Boldyrev, Ivan Troyan, Artem R. Oganov,* and Tian Cui



Cite This: *J. Phys. Chem. Lett.* 2021, 12, 32–40



Read Online

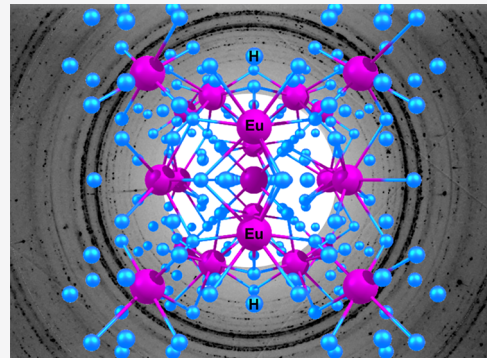
ACCESS |

Metrics & More

Article Recommendations

Supporting Information

ABSTRACT: We conducted a joint experimental–theoretical investigation of the high-pressure chemistry of europium polyhydrides at pressures of 86–130 GPa. We discovered several novel magnetic Eu superhydrides stabilized by anharmonic effects: cubic EuH_9 , hexagonal EuH_9 , and an unexpected cubic ($Pm\bar{3}n$) clathrate phase, Eu_8H_{46} . Monte Carlo simulations indicate that cubic EuH_9 has antiferromagnetic ordering with T_N of up to 24 K, whereas hexagonal EuH_9 and $Pm\bar{3}n\text{-Eu}_8\text{H}_{46}$ possess ferromagnetic ordering with $T_C = 137$ and 336 K, respectively. The electron–phonon interaction is weak in all studied europium hydrides, and their magnetic ordering excludes *s*-wave superconductivity, except, perhaps, for distorted pseudohexagonal EuH_9 . The equations of state predicted within the DFT+U approach ($U - J$ were found within linear response theory) are in close agreement with the experimental data. This work shows the great influence of the atomic radius on symmetry-breaking distortions of the crystal structures of superhydrides and on their thermodynamic stability.



The high-pressure synthesis of new compounds of metal hydrides is a rapidly developing field in view of the unusual chemistry and record-high T_C superconductivity of some hydrides. Some extraordinary compounds, such as CSH_{x_0} ¹ LaH_{10} ,^{2–4} YH_6 and YH_9 ,^{5,6} ThH_9 and ThH_{10} ,⁷ UH_7 ,⁸ CeH_9 ,^{9,10} PrH_9 ,¹¹ and NdH_9 ,¹² have already been synthesized. Some of these hydrides, for example, superhydrides of yttrium,^{5,6} lanthanum,^{3,4} and thorium,⁷ demonstrate remarkable superconductivity. However, magnetic ordering emerging in the hydrides of many *f* metals at low temperatures partially or completely destroys their superconductivity (polyhydrides of praseodymium PrH_9 ,¹¹ and neodymium NdH_9 ,¹²). As we have recently shown for NdH_9 ,¹² taking into account the “spin splitting”¹³ of the electron bands near the Fermi level rules classical superconductivity out because of the high-energy gap that electrons need to overcome for *s* pairing. Nevertheless, the possibility of *d* pairing remains in such materials.

On the other hand, studies of lanthanoid superhydrides are motivated by the need for further development in the description of strongly correlated systems. In the studies of the Pr-H ¹¹ and Nd-H ¹² systems, we have found that the convex hulls obtained with and without the inclusion of spin-orbit coupling (SOC) as well as with or without magnetism and the Hubbard-like correction ($U - J$)¹⁴ differ significantly. In this work, we continue the study of high-pressure chemistry of lanthanoid hydrides focusing on the Eu–H system.

Under normal conditions, europium has the electronic configuration $[\text{Xe}]4f^76s^2$ and an unusually low density and melting point, and a *bcc* lattice with a relatively large cell

parameter of $a = 4.581 \text{ \AA}$.¹⁵ Europium is an anomalous lanthanoid: it is usually divalent and has an abnormally high atomic radius of $\sim 200 \text{ pm}$, about 10% larger than those of Y, Sm, and Gd. Under pressure, it undergoes a series of phase transitions ($bcc \rightarrow hcp \rightarrow C2/c \rightarrow Pnma$)¹⁶ accompanied by the emergence of superconductivity above 80 GPa¹⁷ at 1.8–2.75 K due to the conversion of the Eu atoms from the divalent to the trivalent state with zero magnetic moment. Europium readily reacts with hydrogen, forming $Pnma\text{-EuH}_2$. With excess hydrogen under pressure, the reaction proceeds further, and trivalent tetragonal EuH_{3-x} may be obtained at about 10 GPa.^{18,19} In this work, we continue the study of the Eu–H system at pressures of up to 130 GPa.

Experiment. To investigate the formation of new chemical compounds in the Eu–H system at high pressures, we loaded three high-pressure diamond anvil cells (DAC nos. E1–E3) with metallic europium and sublimated ammonia borane NH_3BH_3 (AB), used as both a source of hydrogen and a pressure-transmitting medium. A tungsten gasket was pressed to $20 \mu\text{m}$. Additional parameters of the high-pressure diamond anvil cells are listed in Supporting Information Table S1.

Received: November 6, 2020

Accepted: December 2, 2020



ACS Publications

© XXXX American Chemical Society

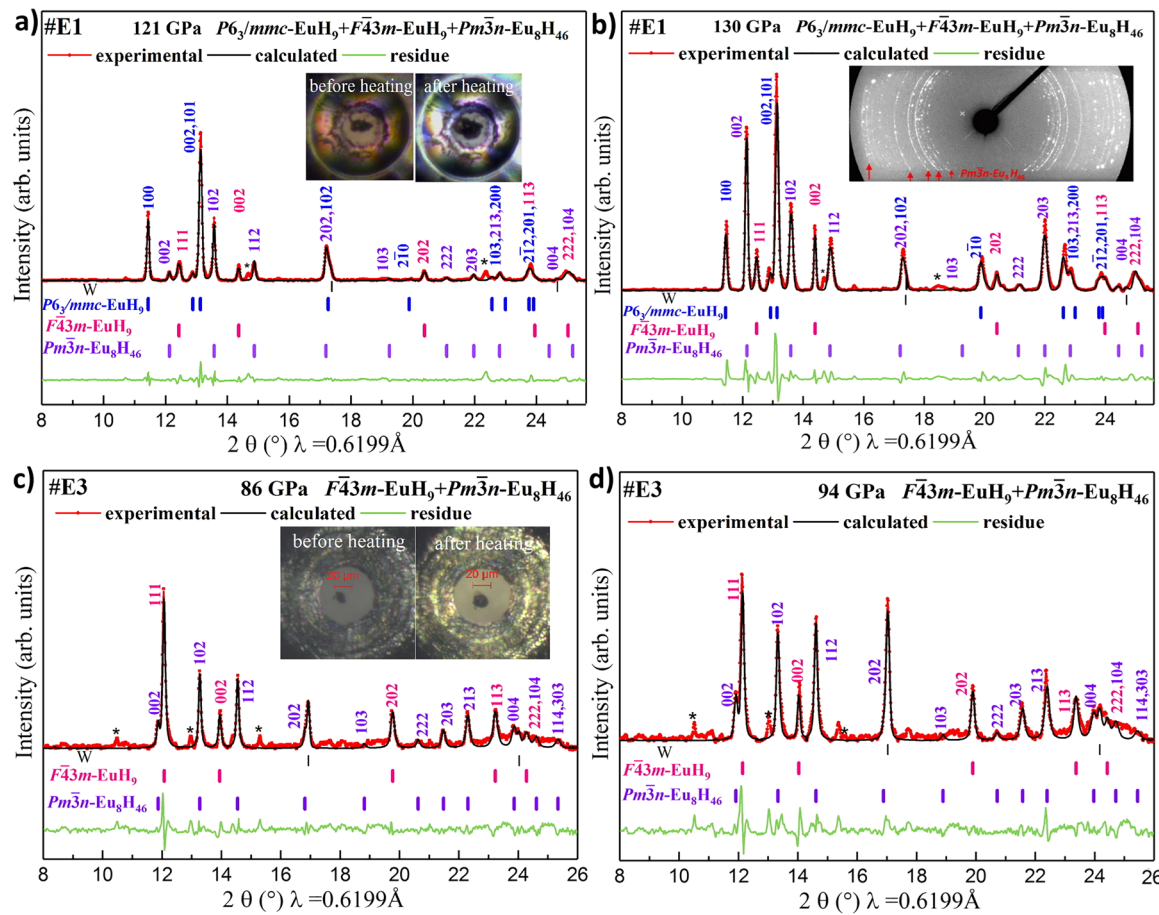


Figure 1. Experimental XRD patterns and Le Bail refinements of Eu hydrides. Le Bail refinements of $\text{F}4\bar{3}m\text{-EuH}_9$, $P6_3/\text{mmc-EuH}_9$, and $\text{Pm}\bar{3}n\text{-Eu}_8\text{H}_{46}$ at (a) 121 GPa and (b) 130 GPa. (Inset) Experimental XRD pattern (cell no. E1). The experimental data, model fit for the structure, and residues are shown in red, black, and green, respectively. Unidentified reflections (possibly $I4/mmm\text{-EuH}_4$) are indicated by asterisks. The reliable parameters for $\text{F}4\bar{3}m\text{-EuH}_9$, $P6_3/\text{mmc-EuH}_9$, and $\text{Pm}\bar{3}n\text{-Eu}_8\text{H}_{46}$ at 121 GPa are $R_p = 21.4\%$ and $R_{wp} = 35.6\%$; at 130 GPa, $R_p = 25.3\%$ and $R_{wp} = 34.6\%$. Le Bail refinements of $\text{F}4\bar{3}m\text{-EuH}_9$ and $\text{Pm}\bar{3}n\text{-Eu}_8\text{H}_{46}$ at (c) 86 GPa and (d) 94 GPa for cell no. E3. The insets of panels a and c of Figure 1 show the sample chamber before and after laser heating of the cell nos. E1 and E3, respectively.

Laser heating of the metal Eu sample in the AB medium at 1600–1800 K for 0.1 s yielded a complex mixture of various europium hydrides observed in DAC nos. E1 and E3. The experimental X-ray diffraction (XRD) patterns are shown in Figure 1. The analysis of the original diffraction images demonstrated the existence of a fine-grained phase with a set of reflections (inset of Figure 1b) that can be indexed in space group $\text{Pm}\bar{3}n$ with $a = 5.858 \text{ \AA}$ and $V = 25.13 \text{ \AA}^3/\text{f.u.}$ at 130 GPa, corresponding to composition EuH_{5+x} , $0 < x < 1$. Similar diffraction patterns have been previously observed in the U–H system⁸ (and attributed to $\beta\text{-UH}_3$) and in the investigation of the Eu–H system by Ma et al.,²⁰ where the authors attributed it to $\text{Pm}\bar{3}n\text{-EuH}_5$.

Two other sets of reflections may be indexed in space group $\text{Fm}\bar{3}m$ or $\text{F}4\bar{3}m$ ($a = 4.947 \text{ \AA}$, $V = 30.27 \text{ \AA}^3/\text{f.u.}$ at 130 GPa) and $P6_3/\text{mmc}$ ($a = 3.591 \text{ \AA}$, $c = 5.509 \text{ \AA}$, $V = 30.76 \text{ \AA}^3/\text{f.u.}$ at 130 GPa), which may be proposed by analogy with the chemistry of the Pr–H¹¹ and Nd–H¹² systems (Figure 1a,b). Both compounds have a cell volume close to that of the Eu/H 1:9 composition. At high pressure (120–130 GPa, DAC no. E1), hexagonal polyhydride EuH_9 is dominant, whereas a small amount of the cubic modification was found, but below 90 GPa the situation is opposite (DAC no. E3, Figure 1c,d). Changing the pressure in cell nos. E1 and E3 allowed us to get the pressure dependence of the cell volume and compare it

with the theoretically calculated equations of state (EoS's) for the obtained phases (Figures 2 and 3). As demonstrated below, this comparison makes it possible to determine the hydrogen content in the discovered compounds and confirm our guesses about EuH_9 . Thus, we found that $\text{F}4\bar{3}m\text{-EuH}_9$ is present in both diamond anvil cells in the pressure range from 86 to 130 GPa, while the formation of $P6_3/\text{mmc-EuH}_9$ requires higher pressure (see also Figure S2).

Additional laser heating of DAC nos. E1 at 130 GPa and E2 at 74 GPa under the same conditions (~1600 K, 0.1 s) with consequent registration of the X-ray diffraction at synchrotron radiation facility SPring-8 (Japan, $\lambda = 0.413 \text{ \AA}$) left the diffraction pattern almost unchanged. The analysis showed that the samples still contained a mixture of cubic and hexagonal EuH_9 and $\text{Pm}\bar{3}n$ phases (Supporting Information Figures S2 and S3 and Figures S12–S15, respectively). The reaction products were unevenly distributed over the volume of the sample: $P6_3/\text{mmc-EuH}_9$ (Supporting Information Figures S2 and S14, high granularity) or $\text{Pm}\bar{3}n\text{-EuH}_{5+x}$ (Supporting Information Figures S12 and S15, low granularity) may dominate other compounds. In DAC no. E2, after compressing to 89 GPa, we mainly found $\text{Pm}\bar{3}n\text{-EuH}_{5+x}$ (Supporting Information Figure S15). Thus, additional laser heating neither improved the purity of the studied mixture nor yielded any

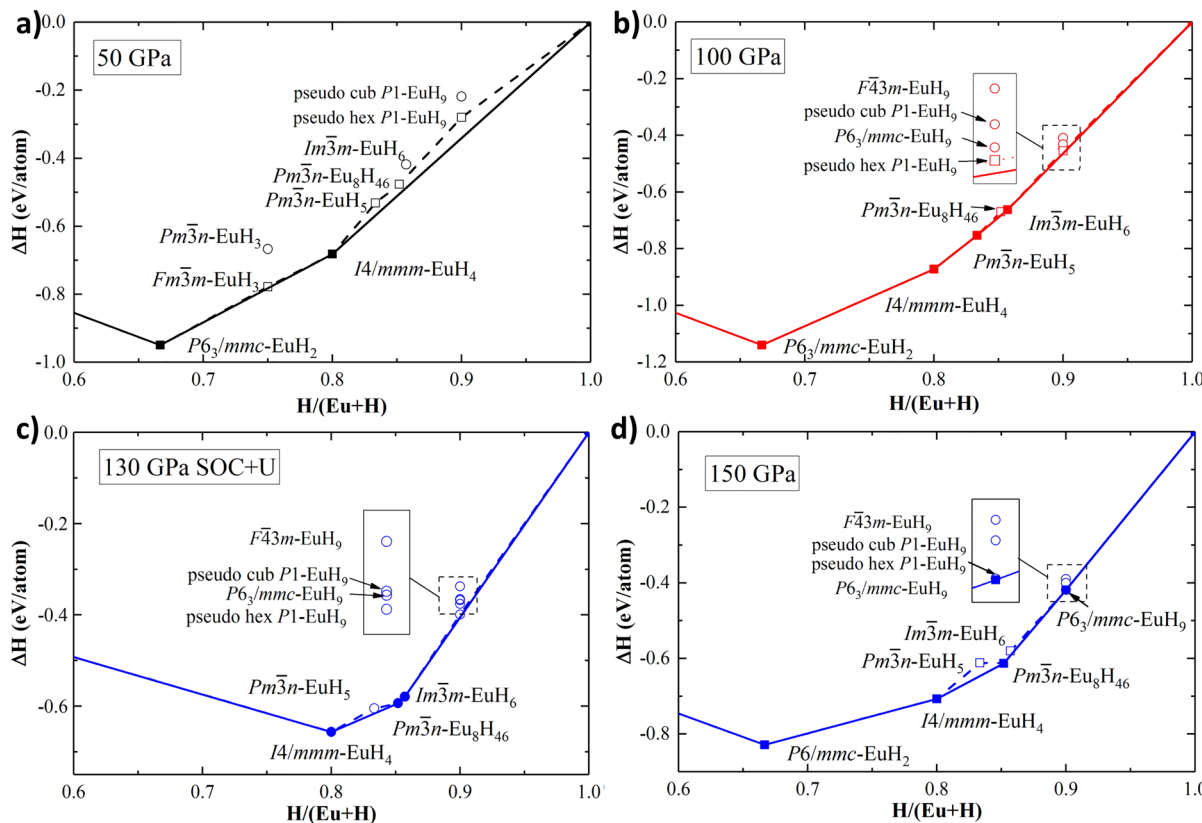


Figure 2. Calculated convex hulls of the Eu–H system at (a) 50, (b) 100, and (d) 150 GPa without SOC and $U - J = 0$ and (c) at 130 GPa with SOC and specific $U - J$ (see Supporting Information, Table S7).

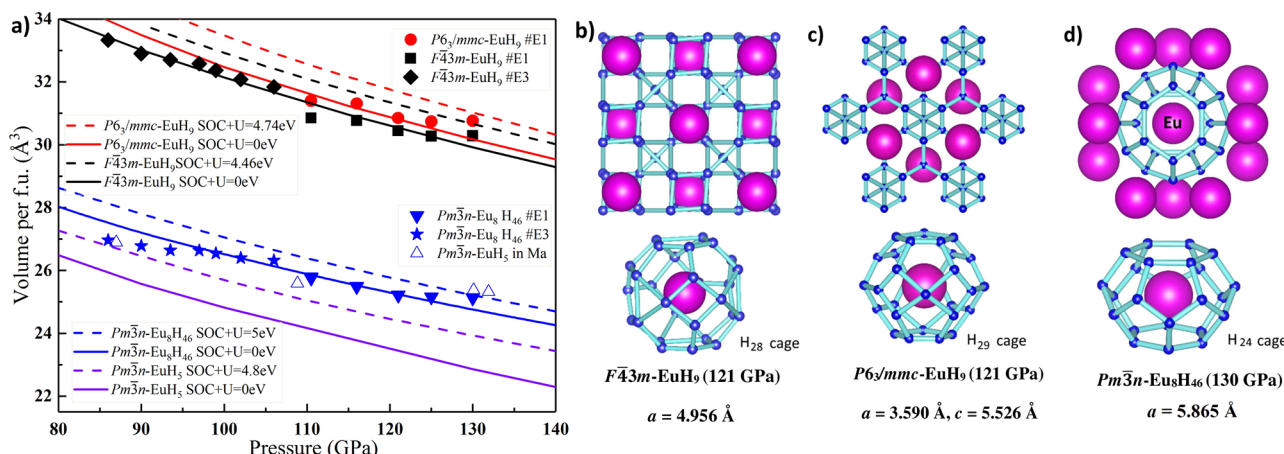


Figure 3. Equations of state and crystal structures of synthesized Eu–H phases. (a) Pressure dependence of volumes of europium hydrides. The theoretical results taking into account SOC are shown by solid ($U - J = 0$ eV) and dashed–dotted ($U - J$ values from Supporting Table S7) lines. The experimental data for EuH_5 from ref 20 are shown by hollow squares. Crystal structures of ideal $F\bar{4}3m$ -EuH₉ (b) and $P6_3/mmc$ -EuH₉ (c) at 121 GPa and $Pm\bar{3}n$ -EuH₈H₄₆ (d) at 130 GPa. Purple and blue spheres represent Eu and H atoms, respectively.

new europium hydrides. The formation and stability of $Pm\bar{3}n$ -EuH_{5+x} was confirmed to at least 89 GPa.

Crystal Structure Search. In order to more accurately establish the composition and compute various physical properties of the synthesized phases, we performed a variable-composition search for stable compounds in the Eu–H system at pressures of 50, 100, 130, and 150 GPa using the Universal Structure Predictor: Evolutionary Xtallography (USPEX) algorithm.^{21–23} The spin–orbit coupling (SOC) and Hubbard-like correction term ($U - J$) were not taken into account in the evolutionary search, but were included when plotting the

convex hulls (Figure 2). The $U - J$ values were found for all novel europium hydrides using the first-principles linear response approach.²⁴ It was possible to compute $U - J$ using VASP^{25–27} by three single-point calculations. The obtained results (Supporting Information Table S7 and Figures S4–S7) are close to $U - J = 4.5$ –5 eV for all studied compounds.

To construct the convex hulls, we used the experimental XRD data from the previous studies of the phase transition of metallic europium. Bi et al.¹⁶ have shown that at 75–92 GPa europium has a $Pnma$ crystal lattice, with $a = 4.977 \text{ \AA}$, $b = 4.264 \text{ \AA}$, $c = 2.944 \text{ \AA}$, and $V = 15.62 \text{ \AA}^3/\text{atom}$ at 75 GPa.

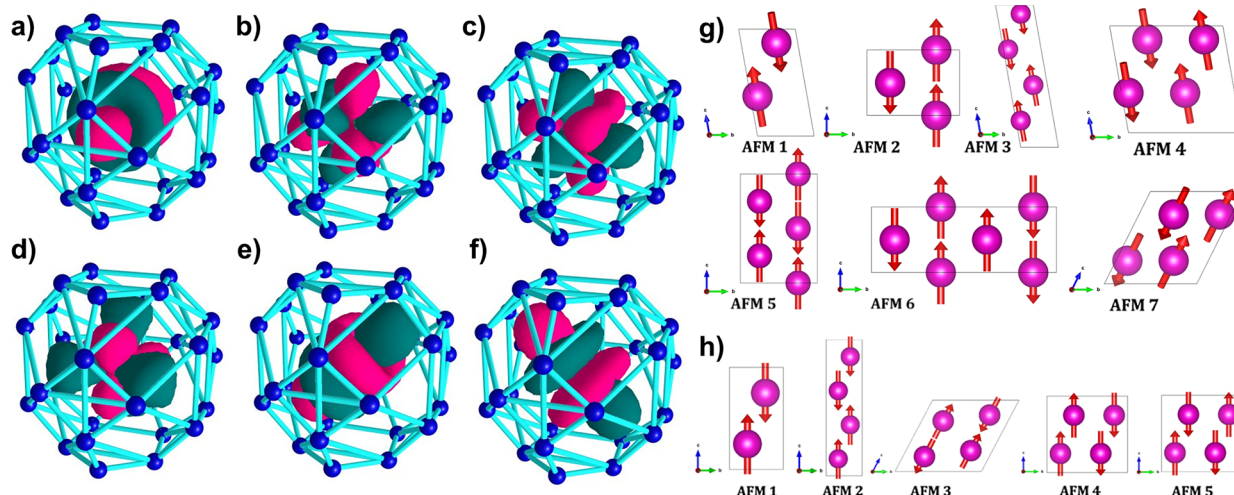


Figure 4. (a–f) Singly occupied F-type superatomic orbitals of EuH_{28}^{19+} (cluster model of $\bar{F}43m\text{-EuH}_9$). (g) Seven trial antiferromagnetic configurations for $F43m\text{-EuH}_9$ (ferromagnetic is trivial) and (h) five trial antiferromagnetic configurations for $P6_3/mmc\text{-EuH}_9$ used in the calculations.

Numerical simulations show that the unit cell volume $V_{Pnma\text{-Eu}}$ shows almost no dependence on the value of $U - J$ in the range of 0–5 eV or on SOC, but the pseudopotential used in calculations strongly affects this volume: $V_{\text{Eu}} = 15.82$ and $13.49 \text{ \AA}^3/\text{atom}$ for 17-electron and 8-electron pseudopotentials, respectively. Because of much better agreement with experiment, the Eu pseudopotential with 17 valence electrons was used in all further calculations.

$I4/mmm\text{-EuH}_4$, a compound from the group of previously found hydrides $I4/mmm\text{-XH}_4$ ($X = \text{Ce, Pr, Nd}$), and $Im\bar{3}m\text{-EuH}_6$ ²⁰ are placed on the convex hull of the Eu–H system in the experimental range of pressure from 100 to 130 GPa (Figure 2). At low pressures of ~ 50 GPa, only $I4/mmm\text{-EuH}_4$ is expected, whereas higher polyhydrides are unstable. The inclusion of SOC and $U - J$ and the analysis of the entropy factor (Supporting Information, Table S9 and Figure S10) do not change the set of stable Eu–H phases, although at 130 GPa and 0 K EuH_9 is slightly (20 meV/atom) above the convex hull. However, the analysis of the equation of state (Figure 3) points to several deviations of $V(P)$ of the predicted europium hydrides from the experimental volumes.

First, the predicted unit cell volume of $Pm\bar{3}n\text{-EuH}_5$ is 22.8 – $23.9 \text{ \AA}^3/\text{f.u.}$ at 130 GPa (without SOC, $U - J = 0$ eV and with SOC and $U - J = 5$ eV, respectively), whereas the experimental value is $25.13 \text{ \AA}^3/\text{f.u.}$, about 1 to 2 \AA^3 higher. The situation holds for other $U - J = 0$ – 7 eV. To solve the problem, get closer to the experimental volume, and find a better structural solution, we increased the hydrogen content x in $Pm\bar{3}n\text{-EuH}_{5+x}$ performing two USPEX searches at 130 GPa with fixed ratios of Eu/H 1:6 and 8:46 (1:5.75, Supporting Information Table S10). The latter composition was proposed by analogy with the well-known $Pm\bar{3}n$ phases of Ge, Si, and Sn clathrates of alkali and alkaline earth metals, such as K_4Ge_{23} , $\text{Rb}_4\text{Ge}_{23}$, $\text{Ba}_8\text{Si}_{46}$, and so forth (so-called Zintl clathrates²⁸). For the former composition, the best solution corresponds to the recently synthesized $Im\bar{3}m\text{-EuH}_6$,²⁰ however, we did not detect this compound in our experiments.

As a result of the second USPEX search, $Pm\bar{3}n\text{-Eu}_8\text{H}_{46}$ was found to be the most stable phase with a cell volume of $25.21 \text{ \AA}^3/\text{Eu}$. This structure features H_{24} cages around each Eu atom (among 24 hydrogens, 8 are closest, with Eu–H distances

below 1.87 \AA). Among the 46 hydrogen atoms in the unit cell, 16 form pairs that can be described as stretched H_2 molecules ($d(\text{H–H}) = 0.99 \text{ \AA}$ vs 0.74 in the free H_2 molecule), and the remaining 30 hydrogen atoms can be described as single atoms (their shortest H–H distance is 1.33 \AA at 130 GPa). This phase corresponds to the experimental XRD and EoS, lies close to the convex hull with and without SOC and $U - J$ (Figure 2), and can explain the experimental data for the “ $Pm\bar{3}n\text{-EuH}_5$ ” phase (Figure 3) obtained by Ma et al.²⁰

Second, ideal $P6_3/mmc\text{-EuH}_9$ is out of the thermodynamic stability area (e.g., Figure 2c). It has been shown recently that similar behavior is observed in the Y–H system,⁶ where ideal $P6_3/mmc\text{-YH}_9$ is also unstable thermodynamically and distorts to stable $P1\text{-Y}_4\text{H}_{36}$ which has almost the same XRD pattern (Figure S1). Using this structure as a prototype, we calculated the enthalpy of similar $P1\text{-Eu}_4\text{H}_{36}$ (which may be relaxed and symmetrized to a pseudohexagonal $Cmcm\text{-EuH}_9$) and found that this distorted structure (Supporting Information Figure S1) is more stable than the ideal $P6_3/mmc\text{-EuH}_9$. Similarly, $\bar{F}43m\text{-EuH}_9$ distorts to form more stable pseudocubic $P1\text{-EuH}_9$.

The calculated unit cell volume of $Fm\bar{3}m\text{-EuH}_{10}$ is 31.8 – $32.4 \text{ \AA}^3/\text{f.u.}$ with $U - J = 0$ and 5 eV, respectively (Supporting Information Figure S8), at 130 GPa, which is 1 to 2 \AA^3 higher than what we found in the experiment for the cubic EuH_x phase (Figures 1 and 3a). Therefore, the existence of $Fm\bar{3}m\text{-EuH}_{10}$, which is isostructural to previously found $Fm\bar{3}m\text{-LaH}_{10}$, is not confirmed by the current experimental data.

It is curious to track how a series of stable europium hydrides change with pressure. At 50 GPa, all europium polyhydrides except EuH_4 are metastable (Figure 2a). An increase in pressure to 100 GPa stabilizes a wide range of polyhydrides, including the above-described $Pm\bar{3}n\text{-EuH}_{46}$, $Im\bar{3}m\text{-EuH}_6$, pseudocubic $P1\text{-EuH}_9$, and pseudohexagonal $P1\text{-EuH}_9$, which is close to $Cmcm$ (Figure 2b). Further increasing the pressure to 150 GPa leads to the stabilization of higher-symmetry structures, and distortions of ideal $\bar{F}43m\text{-EuH}_9$ and $P6_3/mmc\text{-EuH}_9$ cease to play a significant role (Figure 2d). An increase in temperature to 2000 K leads to the destabilization of EuH_9 in favor of EuH_6 , which may explain the unsuccessful experimental attempts to change the phase composition by

additional laser heating ([Supporting Information Figure S10](#)). Anharmonic calculations based on molecular dynamics and machine learning potentials of interatomic interactions (details in the [Supporting Information](#)) show that ideal $P6_3/mmc$ -EuH₉, $F\bar{4}3m$ -EuH₉, and $Pm\bar{3}n$ -Eu₈H₄₆ are dynamically stable, although in the harmonic approximation they should undergo distortions ([Supporting Information Figures S26 and S29–S31](#)). Having predicted the stable compositions and structures of europium hydrides, we now want to gain insight into their nature.

Superatomic Orbitals and Chemical Bonding. The description of electronic structure in terms of delocalized canonical orbitals is almost completely devoid of an explicit chemical bonding picture of a given system. To understand the chemical bonding in europium polyhydrides, we first analyzed model clusters (blocks separated from the infinite crystal lattice) via the adaptive natural density partitioning (AdNDP) algorithm.²⁹ The AdNDP is a localization technique that follows general ideas of the natural bond orbital (NBO) analysis proposed by Weinhold and Landis.³⁰ The main advantage of this method is the possibility to represent a chemical bonding pattern in terms of both Lewis bonding elements (lone pairs, two-center two-electron (2c–2e) bonds) and delocalized bonding elements (nc –2e bonds) by partial diagonalization of the one-body reduced density matrix. This technique is widely used in materials science and in describing various Zintl clusters.^{31–33} The chemical bonding analysis can offer insights into the reasons for the stability, electronic properties, magnetism, and chemical activity of investigated systems. It has been shown that the chemical bonding analysis of cluster models qualitatively agrees with the analysis of solid-state structures.^{34–37} In this work, we used EuH₂₇¹⁸⁺ as a model of $P6_3/mmc$ -EuH₉, EuH₂₄¹⁷⁺ as a model of $Pm\bar{3}n$ -Eu₈H₄₆, and EuH₂₈¹⁹⁺ as a model of $F\bar{4}3m$ -EuH₉ ([Figure 4](#)). Charges were chosen so as to adjust the overall number of electrons per Eu atom in a studied fragment and consider those electrons shared between the cluster and the neighboring atoms.

Starting our search from localized bonding elements such as 2c–2e, 3c–3e, and so forth, we found no highly occupied localized bonds in the present structures. Because of the absence of highly occupied localized bonding elements, the model clusters could be completely described in terms of fully delocalized canonical molecular orbitals (MOs). As was expected, for such sphere-like clusters, the canonical MOs mimic the spherical harmonics forming so-called superatomic orbitals.³⁸ Further analysis of the superatomic orbitals of corresponding clusters reveals that unpaired electrons are located mostly on the F-type orbitals ([Figure 4a–f](#)), whereas the S-, P-, and D-type orbitals are doubly occupied.

Following the analysis of the model clusters, we performed the solid-state AdNDP (SSAdNDP) calculations for ideal cubic and hexagonal EuH₉ and Zintl-like clathrate $Pm\bar{3}n$ -Eu₈H₄₆. Such an analysis was first implemented for polyhydrides in the current work. SSAdNDP revealed the same bonding picture as was found in the model clusters. A cognate pattern could also be seen in the comparison of the electron localization function (ELF) plots of the solid-state structures and model clusters ([Supporting Information Figure S19](#)). The corresponding occupancies of valence superatomic orbitals are presented in [Supporting Information Table S6](#). For all europium polyhydride structures, there are seven almost ideally (1.00 e , where e is the elementary charge) singly occupied superatomic F orbitals, which are responsible for the magnetic properties.

The corresponding nc –2e occupancy numbers (where n is the number of hydrogen atoms in the cage) of superatomic D and P orbitals are (1.72–1.39) e for $P6_3/mmc$ -EuH₉, (1.17–1.09) e for $Pm\bar{3}n$ -Eu₈H₄₆, and (1.57–1.38) e for $F\bar{4}3m$ -EuH₉. Because of the delocalization of conducting electrons, which is common for metals,³⁹ these values are about (0.3–0.9) e lower than those that we found for clusters.

To understand the charge distribution in the studied structures, Bader charge analysis was performed.⁴⁰ In all structures, the Eu atom bears a positive charge of +1.15 e to +0.89 e , whereas a partial negative charge of –0.31 e to –0.08 e was found for all hydrogen atoms. This behavior is common for metal hydrides, and similar results have been found in previous works. The average Bader charges are presented in [Supporting Information Table S18](#).

Both cubic and hexagonal EuH₉ as well as Eu₈H₄₆ demonstrate a large magnetic moment (absolute value) in the unit cell ([Figure S7](#)), slightly decreasing as the pressure increases. At 100 GPa, the magnetic moment of EuH₉ is 5.96 μ_B per Eu atom for the $P6_3/mmc$ modification, 6.32 μ_B per Eu atom for the $Pm\bar{3}n$ -Eu₈H₄₆ structure, and about 5.88 μ_B per Eu atom for cubic EuH₉. The magnetization arises mostly from the f electrons of the Eu atoms. We observed the same behavior for the corresponding clusters ([Supporting Information Table S5](#)): the ground spin state of EuH₂₇¹⁸⁺ and EuH₂₄¹⁷⁺ is nonet ($S_{\text{total}} = 4$), whereas for EuH₂₈¹⁹⁺ the ground spin state is septet ($S_{\text{total}} = 3$).

We performed a comparative analysis of superatomic orbitals of europium hydrides, recently synthesized cubic and hexagonal PrH₉,¹¹ and hexagonal NdH₉,¹² ([Supporting Information Table S17](#)). For PrH₉, the shapes of five obtained nc –2e bonds do not completely correspond to the D type: two orbitals have a D-type nature, and the three other nc –2e bonds have the F-type nature. This probably happens because of the ambiguous behavior of f and d orbitals of lanthanoids. Similar behavior—the mixing of F and D orbitals—was also observed for the molecular clusters of these hydrides and for the NdH₂₄¹⁶⁺ cluster, which has D-type and F-type orbitals with very similar energies.

The analysis of MOs revealed that all clusters could be described within the superatomic concept, according to which the most stable clusters emerge from completely filled superatomic shells. However, CeH₂₉²⁰⁺ ([Supporting Information Figure S18](#)) has an additional 2P electron that contradicts this concept. We believe that this P electron plays an important role in the metallic and superconducting ($T_C \approx 110$ K (unpublished)) properties of cerium polyhydrides as was previously shown for LaH₁₀.⁴¹ The overall approach of the localization of superatomic orbitals in hydrogen cages could also be extended to other superconducting polyhydrides. For example, strong localization of the multicenter bond was found for H₃₂ cages present in LaH₁₀ and YH₁₀ superconductors. As in the case of Ce polyhydride, 2P electrons in these structures were found to have relatively high occupation numbers. The 2S superatomic orbital, which is present in clusters, is absent in solid-state superatoms. We think that these two electrons, localized on the H cage of clusters, may participate in metallic interactions and cannot be localized via the SSAdNDP technique. The detailed comparison of occupancies of the superatomic orbitals in different polyhydrides is presented in [Supporting Information Table S17](#).

Magnetic Structure. To analyze the magnetic structure of europium hydrides, we studied a series of ferromagnetic (FM)

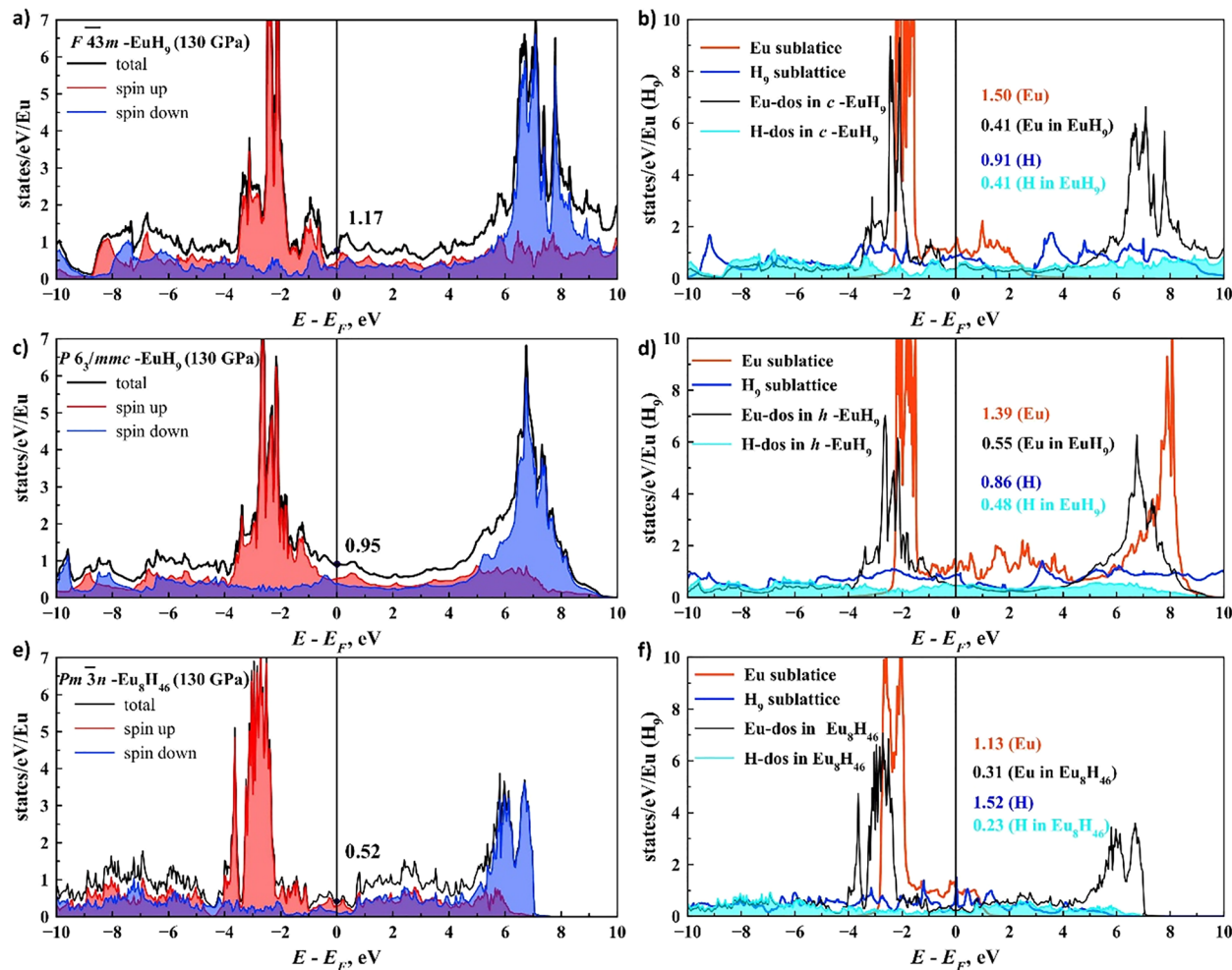


Figure 5. Electron density of states (DOS) of europium hydrides at 130 GPa. (a, c, e) Contributions of different spin orientations to the total DOS. (b, d, f) Contributions of the Eu and H atoms to the total DOS. The DOS of the Eu sublattice separated from hydrogen at 130 GPa is shown in red; the DOS of the H₉ sublattice separated from the Eu atoms at 130 GPa is shown in blue.

and antiferromagnetic (AFM) configurations. The enthalpies of the optimized structures are presented in [Supporting Information Table S11](#). During the calculation, the ideal cubic and hexagonal structures of hydrides are distorted into more stable low-symmetry pseudocubic and pseudohexagonal modifications. Most of these distorted structures have XRD pattern close to the ideal ones. To simplify the magnetic calculations, in several cases we used high-symmetry EuH₉ prototypes ($F\bar{4}3m$ and $P6_3/mmc$) instead of thermodynamically more stable distorted $P1$ -Eu₄H₃₆. The magnetic structure of the pseudohexagonal $Cmcm$ -EuH₉ has nevertheless been studied in detail ([Supporting Information](#)).

The most stable collinear magnetic state of $F\bar{4}3m$ -EuH₉ is AFM 1, which distorts to $P1$ during relaxation. The second most stable configuration is AFM 3, which distorts to $Imm2$. Finally, among the magnetic states that preserve the original ideal $F\bar{4}3m$ symmetry, the most stable is AFM 2. The same is observed for $P6_3/mmc$ -EuH₉. The most stable collinear magnetic state is AFM 3, but during relaxation the hexagonal structure is distorted and transformed to pseudohexagonal $Cmcm$, which lies on the convex hull ([Figures 2 and 4](#)). The second most stable configuration is AFM 4, which distorts to $C2$. Among the magnetic states that preserve the ideal $P6_3/mmc$ symmetry, the most stable is FM. The most stable collinear configuration for Eu₈H₄₆ is FM. Unlike the EuH₉,

phases, the magnetic configurations of Eu₈H₄₆ do not show significant distortions from the ideal $Pm\bar{3}n$ geometry after relaxation.

For each of our three phases, we used the relaxed geometries of the most stable magnetic states to study magnetic anisotropy by running calculations with SOC. We computed the single-point enthalpy of these structures in both the FM and in one AFM state, with the magnetic moments aligned along different directions (x , y , z , xy , xz , yz , and xyz). The results are summarized in [Supporting Information Table S12](#). We expect a small amount of magnetic anisotropy for all phases with EuH₉ stoichiometry, for which we identified the most stable orientation of the magnetic moments. We do not expect any magnetic anisotropy in $Pm\bar{3}n$ -Eu₈H₄₆ because different orientations of the magnetic moments have almost the same enthalpy up to the numerical errors.

To study the Néel and Curie temperatures of $F\bar{4}3m$ -EuH₉, $P6_3/mmc$ -EuH₉, and $Pm\bar{3}n$ -Eu₈H₄₆, we modeled the magnetic interaction within the Ising Hamiltonian and obtained the critical temperatures for both EuH₉ and Eu₈H₄₆ in our Heisenberg model from a Monte Carlo simulation as implemented in the VAMPIRE code⁴² ([Supporting Information Table S14](#)). We obtained the critical temperature $T_N = 24$ K for cubic EuH₉, while hexagonal EuH₉ and $Pm\bar{3}n$ -Eu₈H₄₆

possess ferromagnetic ordering with $T_C = 137$ and 336 K, respectively.

Electron–Phonon Interaction. Strong electron–phonon coupling (EPC) is expected for lanthanides and their polyhydrides under pressure. It has been shown for superhydrides of Ce,^{9,10} Pr,^{11,43} and Nd^{12,44} that the superconducting (SC) properties and the strength of the electron–phonon interactions decrease as the number of f electrons increases and manifestations of magnetism become more pronounced.

The numerical analysis using the UppSC code¹² performed for hexagonal NdH₉ (120 GPa)¹² showed that if the effective spin splitting in the band structure $h(k) = [\xi_{\uparrow}(k) - \xi_{\downarrow}(k)]/2$, where $\xi(k)$ is the spin-resolved electron dispersion, is about 0.5 eV or higher then superconductivity will be completely suppressed at all $\mu^* \geq 0$. We found that a similar spin splitting gap reaches 4–4.5 eV in both EuH₉ and Eu₈H₄₆ (Figure 5a,c,e), which is 2 orders of magnitude larger than for all known SC gaps. This fact excludes singlet superconductivity and s pairing in europium hydrides.

Despite this pessimistic conclusion, we estimated the parameters of the electron–phonon interaction in europium hydrides as if magnetism were absent. The results show that the distorted H sublattice in both modifications of EuH₉ could be a superconductor with a T_C of up to 21 K ($\mu^* = 0.1$), an EPC coefficient $\lambda = 0.61$, and $\omega_{\log} = 836$ K for hexagonal EuH₉, and $T_C = 27$ K and $\lambda = 0.51$ for cubic EuH₉. Compared with LaH₁₀ ($T_C \geq 250$ K^{3,4}), this indicates the enormous role played by the metal atom (even in the absence of magnetism) and surprisingly different electron–phonon coupling properties of the otherwise very similar lanthanoids. The crucial role of the hydride-forming element and its electronic structure in the T_C of the hydride has been discussed before.⁴⁴

The projection of the total density of states of both EuH₉ on the H atoms, $N_H(E_F)$, is 0.41–0.48 states/eV/Eu (Figure 5b,d,f) at 130 GPa. An estimate of the logarithmic frequency made on the basis of the experimental equation of state yields $\omega_{\log} = 975$ –1060 K for EuH₉ at 100 GPa, agreeing with calculations. Both of these factors would be favorable to superconductivity if electron–phonon coupling were stronger and if there were no magnetic ordering. An exception may exist for pseudohexagonal Cmcm-EuH₉, which does not exhibit magnetism at finite temperatures (Supporting Information).

Compared to PrH₉ and NdH₉, f electrons in europium hydrides are localized much deeper (−2 eV) below the Fermi level, and $N(E_F)$ is ∼0.95–1.17 states/eV/Eu in EuH₉, similar to the values for LaH₁₀ and YH₆, with a high contribution of the H sublattice (∼50% of $N(E_F)$). If we consider the metal and hydrogen sublattices in EuH₉ separately, disregarding the interaction between them (Figure 5b,d,f), then we will see that the influence of this interaction is completely negative for both $N_H(E_F)$ and $N_{Eu}(E_F)$, which decrease by 1.8–2-fold. The calculation of the superconducting properties of the formally separated Eu and H sublattices of F43m-EuH₉ at 130 GPa shows that the critical temperature of hydrogen (“H₉”) in the cubic sublattice reaches 150–200 K, while interaction with Eu leads to about a 5 times lower T_C (EuH₉) of ∼27 K. Thus, the metal lattice plays the role of a stabilizer of metallic hydrogen but reduces the density of states $N_H(E_F)$ at the Fermi level and the critical temperature of superconductivity.

In conclusion, continuing the studies of the stabilization of metallic hydrogen in compressed metal–hydrogen systems, we synthesized three novel europium superhydrides with probably slightly distorted structures due to the abnormally large radius

of the Eu atom: P6₃/mmc-EuH₉, F43m-EuH₉, and an unexpected clathrate phase, Pm3n-Eu₈H₄₆. The discovered cubic and hexagonal modifications of EuH₉ are the new members of the nonahydride family, which currently includes the polyhydrides of Th, U, Y, Ce, Pr, and Nd. Similar to the Nd–H system, all europium hydrides are magnetic and strongly correlated systems with a significant contribution of the SOC interaction. They possess antiferromagnetic (cubic EuH₉) or ferromagnetic (hexagonal EuH₉, Eu₈H₄₆) ordering with $T_{N,C} \approx 24$ –336 K. Although the projection of the DOS on the H sublattice in both phases of EuH₉ is similar to that of high- T_C superconducting hydrides, such as LaH₁₀ and YH₆, the electron–phonon coupling is weak. Magnetic order and a large effective spin splitting (>4 eV) in the electron band structure of EuH₉ make classical s-wave superconductivity impossible. An exception may take place for pseudohexagonal Cmcm-EuH₉, which does not exhibit magnetism at finite temperatures.

The chemical bonding analysis was implemented for polyhydrides for the first time. The analysis points to the contribution of 2P superatomic electrons as an important distinguishing feature in determining high-temperature superconductivity. It was found that the superatomic description of polyhydrides could be extended to other important superconductors, such as LaH₁₀ and YH₆.

By analyzing the whole series of La–Ce–Pr–Nd–Eu superhydrides, we conclude that the role of magnetism is gradually increasing in this row, which leads to the suppression of s-wave superconductivity. Most of the higher superhydrides of these metals have antiferromagnetic ordering, whereas the lower hydrides have ferromagnetic ordering. Europium hydrides, in addition to Y₄H₃₆ and BaH₁₂, give us yet another indication of the great role of distortions of the ideal hexagonal and cubic structures in their stabilization. Without considering these distortions, a theoretical explanation of the thermodynamic stability of europium superhydrides would be impossible.

ASSOCIATED CONTENT

Supporting Information

The Supporting Information is available free of charge at <https://pubs.acs.org/doi/10.1021/acs.jpcllett.0c03331>.

Detailed descriptions of the used experimental and computational methods; structural information on the predicted and synthesized structures; additional data for the Le Bail refinements; information on the magnetic structure, natural population analysis, electronic structure, phonons, anharmonic calculations, and elastic properties (PDF)

AUTHOR INFORMATION

Corresponding Authors

Xiaoli Huang – State Key Laboratory of Superhard Materials, College of Physics, Jilin University, Changchun 130012, China;  orcid.org/0000-0001-9628-5618; Email: huangxiaoli@jlu.edu.cn

Artem R. Oganov – Skolkovo Institute of Science and Technology, Skolkovo Innovation Center, Moscow 143026, Russia;  orcid.org/0000-0001-7082-9728; Email: a.oganov@skoltech.ru

Authors

Dmitrii V. Semenok – Skolkovo Institute of Science and Technology, Skolkovo Innovation Center, Moscow 143026, Russia; orcid.org/0000-0002-1374-9091

Di Zhou – State Key Laboratory of Superhard Materials, College of Physics, Jilin University, Changchun 130012, China

Alexander G. Kvashnin – Skolkovo Institute of Science and Technology, Skolkovo Innovation Center, Moscow 143026, Russia; orcid.org/0000-0002-0718-6691

Michele Galasso – Skolkovo Institute of Science and Technology, Skolkovo Innovation Center, Moscow 143026, Russia

Ivan A. Kruglov – Moscow Institute of Physics and Technology, Dolgoprudny 141700, Russia; Dukhov Research Institute of Automatics (VNIIA), Moscow 127055, Russia; orcid.org/0000-0003-1786-9282

Anna G. Ivanova – Shubnikov Institute of Crystallography, Federal Scientific Research Center Crystallography and Photonics, Russian Academy of Sciences, Moscow 119333, Russia

Alexander G. Gavriliuk – Shubnikov Institute of Crystallography, Federal Scientific Research Center Crystallography and Photonics, Russian Academy of Sciences, Moscow 119333, Russia; IC RAS Institute for Nuclear Research, Russian Academy of Sciences, Moscow 117312, Russia; orcid.org/0000-0003-0604-586X

Wuhao Chen – State Key Laboratory of Superhard Materials, College of Physics, Jilin University, Changchun 130012, China

Nikolay V. Tkachenko – Department of Chemistry and Biochemistry, Utah State University, Logan, Utah 84322-0300, United States; orcid.org/0000-0002-7296-4293

Alexander I. Boldyrev – Department of Chemistry and Biochemistry, Utah State University, Logan, Utah 84322-0300, United States; orcid.org/0000-0002-8277-3669

Ivan Troyan – Shubnikov Institute of Crystallography, Federal Scientific Research Center Crystallography and Photonics, Russian Academy of Sciences, Moscow 119333, Russia

Tian Cui – State Key Laboratory of Superhard Materials, College of Physics, Jilin University, Changchun 130012, China; School of Physical Science and Technology, Ningbo University, Ningbo 315211, China; orcid.org/0000-0002-9664-848X

Complete contact information is available at:

<https://pubs.acs.org/10.1021/acs.jpcllett.0c03331>

Author Contributions

D.V.S., D.Z., and A.G.K. contributed equally to this work. X.H. and A.R.O. conceived this project. D.Z., D.V.S., I.A.T., A.G.I., A.G.G., and X.H. performed the experiment. D.V.S., D.Z., A.R.O., and T.C. prepared the theoretical calculations and analysis. M.G. studied the magnetic properties. X.H., D.Z., D.V.S., M.G., A.R.O., and T.C. wrote and revised the paper. All authors discussed the results and offered useful ideas.

Notes

The authors declare no competing financial interest.

ACKNOWLEDGMENTS

The authors express their gratitude to the staff of the BL10XU (High Pressure Research) station of the SPring-8 synchrotron research facilities, especially Saori Kawaguchi (JASRI) for the

tremendous assistance in the use of the station's equipment before and after the experiment (proposal No. 2019B1476). We also thank the staffs of the BL1SU station of Shanghai and the 4W2 station of the Beijing Synchrotron Radiation Facilities. This work was supported by the National Key R&D Program of China (grant no. 2018YFA0305900), the National Natural Science Foundation of China (grant nos. 11974133 and 51720105007), the National Key Research and Development Program of China (grant no. 3382016YFB0201204) and the Program for Changjiang Scholars and the Innovative Research Team in University (grant no. IRT_15R23). I.T. and A.G.I. thank the the Russian Science Foundation (project no. 19-12-00414) for support of this work. A.R.O. thanks the Russian Science Foundation (grant no. 19-72-30043). A.G.K. and D.V.S. thank the Russian Foundation for Basic Research, grant no. 19-03-00100. D.V.S. thank the Russian Foundation for Basic Research (grant no. 20-32-90099). A.R.O and D.V.S. thank the Ministry of Science and Higher Education (agreement no. 075-15-2020-808). N.V.T. and A.I.B. also thank the U.S. National Science Foundation (grant CHE-1664379) and the resources from the Center for High Performance Computing at the University of Utah. A.G.G. acknowledges support from the Center for Collective Use Accelerator, Center for Neutron Research of the Structure of Substance and Nuclear Medicine of the INR RAS. We thank Igor Grishin (Skoltech) for proofreading the manuscript.

REFERENCES

- (1) Snider, E.; Dasenbrock-Gammon, N.; McBride, R.; Debessai, M.; Vindana, H.; Venkatasamy, K.; Lawler, K. V.; Salamat, A.; Dias, R. P. Room-temperature superconductivity in a carbonaceous sulfur hydride. *Nature* **2020**, *586*, 373–377.
- (2) Geballe, Z. M.; Liu, H.; Mishra, A. K.; Ahart, M.; Somayazulu, M.; Meng, Y.; Baldini, M.; Hemley, R. J. Synthesis and Stability of Lanthanum Superhydrides. *Angew. Chem., Int. Ed.* **2018**, *57*, 688–692.
- (3) Drozdov, A. P.; Kong, P. P.; Minkov, V. S.; Besedin, S. P.; Kuzovnikov, M. A.; Mozaffari, S.; Balicas, L.; Balakirev, F. F.; Graf, D. E.; Prakapenka, V. B.; et al. Superconductivity at 250 K in lanthanum hydride under high pressures. *Nature* **2019**, *569*, 528–531.
- (4) Somayazulu, M.; Ahart, M.; Mishra, A. K.; Geballe, Z. M.; Baldini, M.; Meng, Y.; Struzhkin, V. V.; Hemley, R. J. Evidence for Superconductivity above 260 K in Lanthanum Superhydride at Megabar Pressures. *Phys. Rev. Lett.* **2019**, *122*, 027001.
- (5) Kong, P. P.; Minkov, V. S.; Kuzovnikov, M. A.; Besedin, S. P.; Drozdov, A. P.; Mozaffari, S.; Balicas, L.; Balakirev, F. F.; Prakapenka, V. B.; Greenberg, E., et al. Superconductivity up to 243 K in yttrium hydrides under high pressure. *arXiv:1909.10482* 2019.
- (6) Troyan, I. A.; Semenok, D. V.; Kvashnin, A. G.; Ivanova, A. G.; Prakapenka, V. B.; Greenberg, E.; Gavriliuk, A. G.; Lyubutin, I. S.; Struzhkin, V. V.; Oganov, A. R. Synthesis and Superconductivity of Yttrium Hexahydride $\text{Im}\text{-}3\text{m}$ - YH_6 . *arXiv:1908.01534v1* 2019.
- (7) Semenok, D. V.; Kvashnin, A. G.; Ivanova, A. G.; Svitlyk, V.; Fominski, V. Y.; Sadakov, A. V.; Sobolevskiy, O. A.; Pudalov, V. M.; Troyan, I. A.; Oganov, A. R. Superconductivity at 161K in thorium hydride ThH_{10} : Synthesis and properties. *Mater. Today* **2020**, *33*, 36–44.
- (8) Kruglov, I. A.; Kvashnin, A. G.; Goncharov, A. F.; Oganov, A. R.; Lobanov, S. S.; Holtgrewe, N.; Jiang, S. Q.; Prakapenka, V. B.; Greenberg, E.; Yanilkin, A. V. Uranium polyhydrides at moderate pressures Predict: Prediction, synthesis, and expected superconductivity. *Sci. Adv.* **2018**, *4*, No. eaat9776.
- (9) Salke, N. P.; Esfahani, M. M. D.; Zhang, Y.; Kruglov, I. A.; Zhou, J.; Wang, Y.; Greenberg, E.; Prakapenka, V. B.; Liu, J.; Oganov, A. R.; et al. Synthesis of clathrate cerium superhydride CeH_9 at 80 GPa with anomalously short H-H distance. *Nat. Commun.* **2019**, *10*, 4453.

- (10) Li, X.; Huang, X.; Duan, D.; Pickard, C. J.; Zhou, D.; Xie, H.; Zhuang, Q.; Huang, Y.; Zhou, Q.; Liu, B.; et al. Polyhydride CeH₉ with an atomic-like hydrogen clathrate structure. *Nat. Commun.* **2019**, *10*, 3461.
- (11) Zhou, D.; Semenok, D. V.; Duan, D.; Xie, H.; Huang, X.; Chen, W.; Li, X.; Liu, B.; Oganov, A. R.; Cui, T. Superconducting Praseodymium Superhydrides. *Sci. Adv.* **2020**, *6*, No. eaax6849.
- (12) Zhou, D.; Semenok, D. V.; Xie, H.; Huang, X.; Duan, D.; Aperis, A.; Oppeneer, P. M.; Galasso, M.; Kartsev, A. I.; Kvashnin, A. G.; et al. High-Pressure Synthesis of Magnetic Neodymium Polyhydrides. *J. Am. Chem. Soc.* **2020**, *142*, 2803–2811.
- (13) Aperis, A.; PabloMaldonado Oppeneer, P. M. Ab initio theory of magnetic-field-induced odd-frequency two-band superconductivity in MgB₂. *Phys. Rev. B: Condens. Matter Mater. Phys.* **2015**, *92*, 054516.
- (14) Dudarev, S. L.; Botton, G. A.; Savrasov, S. Y.; Humphreys, C. J.; Sutton, A. P. Electron-energy-loss spectra and the structural stability of nickel oxide: An LSDA+U study. *Phys. Rev. B: Condens. Matter Mater. Phys.* **1998**, *57*, 1505–1509.
- (15) Greenwood, N. N.; Earnshaw, A. *Chemistry of the Elements*; Pergamon Press: 1984.
- (16) Bi, W.; Meng, Y.; Kumar, R. S.; Cornelius, A. L.; Tipton, W. W.; Hennig, R. G.; Zhang, Y.; Chen, C.; Schilling, J. S. Pressure-induced structural transitions in europium to 92 GPa. *Phys. Rev. B: Condens. Matter Mater. Phys.* **2011**, *83*, 104106.
- (17) Debessai, M.; Matsuoka, T.; Hamlin, J. J.; Schilling, J. S.; Shimizu, K. Pressure-induced superconducting state of europium metal at low temperatures. *Phys. Rev. Lett.* **2009**, *102*, 197002.
- (18) Saitoh, H.; Machida, A.; Matsuoka, T.; Aoki, K. Phase diagram of the Eu-H system at high temperatures and high hydrogen pressures. *Solid State Commun.* **2015**, *205*, 24–27.
- (19) Matsuoka, T.; Fujihisa, H.; Hirao, N.; Ohishi, Y.; Mitsui, T.; Masuda, R.; Seto, M.; Yoda, Y.; Shimizu, K.; Machida, A.; et al. Structural and valence changes of europium hydride induced by application of high-pressure H(2). *Phys. Rev. Lett.* **2011**, *107*, 025501.
- (20) Ma, L.; Liu, G.; Wang, Y.; Zhou, M.; Liu, H.; Peng, F.; Wang, H.; Ma, Y. Experimental Syntheses of Sodalite-like Clathrate EuH₆ and EuH₉ at Extreme Pressures. *arXiv:2002.09900* 2020.
- (21) Oganov, A. R.; Lyakhov, R. O.; Valle, M. How Evolutionary Crystal Structure Prediction Works-and Why. *Acc. Chem. Res.* **2011**, *44*, 227–237.
- (22) Oganov, A. R.; Glass, C. W. Crystal structure prediction using ab initio evolutionary techniques: Principles and applications. *J. Chem. Phys.* **2006**, *124*, 244704.
- (23) Lyakhov, A. O.; Oganov, A. R.; Stokes, H. T.; Zhu, Q. New developments in evolutionary structure prediction algorithm USPEX. *Comput. Phys. Commun.* **2013**, *184*, 1172–1182.
- (24) Giannozzi, P.; Baroni, S.; Bonini, N.; Calandra, M.; Car, R.; Cavazzoni, C.; Ceresoli, D.; Chiarotti, G. L.; Cococcioni, M.; Dabo, I.; et al. QUANTUM ESPRESSO: a modular and open-source software project for quantum simulations of materials. *J. Phys.: Condens. Matter* **2009**, *21*, 395502.
- (25) Kresse, G.; Hafner, J. Ab initio molecular dynamics for liquid metals. *Phys. Rev. B: Condens. Matter Mater. Phys.* **1993**, *47*, 558–561.
- (26) Kresse, G.; Hafner, J. Ab initiomolecular-dynamics simulation of the liquid-metal-amorphous-semiconductor transition in germanium. *Phys. Rev. B: Condens. Matter Mater. Phys.* **1994**, *49*, 14251–14269.
- (27) Kresse, G.; Hafner, J. Efficient iterative schemes for ab initio total-energy calculations using a plane-wave basis set. *Phys. Rev. B: Condens. Matter Mater. Phys.* **1996**, *54*, 11169.
- (28) King, R. B. *Encyclopedia of Inorganic Chemistry*, 2nd ed.; Wiley: Hoboken, NJ, 2005; Vol. 10.
- (29) Tkachenko, N. V.; Boldyrev, A. I. Chemical bonding analysis of excited states using the adaptive natural density partitioning method. *Phys. Chem. Chem. Phys.* **2019**, *21*, 9590–9596.
- (30) Weinhold, F.; Landis, C. R. *Valency and Bonding: A Natural Bond Orbital Donor-Acceptor Perspective*; Cambridge University Press: Cambridge, U.K., 2005.
- (31) Tkachenko, N. V.; Song, B.; Steglenko, D.; Minyaev, R. M.; Yang, L.-M.; Boldyrev, A. I. Computational Prediction of the Low-Temperature Ferromagnetic Semiconducting 2D SiN Monolayer. *Phys. Status Solidi B* **2020**, *257*, 1900619.
- (32) Steglenko, D. V.; Tkachenko, N. V.; Boldyrev, A. I.; Minyaev, R. M.; Minkin, V. I. Stability, electronic, and optical properties of two-dimensional phosphoborane. *J. Comput. Chem.* **2020**, *41*, 1456–1463.
- (33) Dong, X.; Oganov, A. R.; Goncharov, A. F.; Stavrou, E.; Lobanov, S.; Saleh, G.; Qian, G.-R.; Zhu, Q.; Gatti, C.; Deringer, V. L.; et al. A stable compound of helium and sodium at high pressure. *Nat. Chem.* **2017**, *9*, 440–445.
- (34) Popov, I. A.; Bozhenko, K. V.; Boldyrev, A. I. Is graphene aromatic? *Nano Res.* **2012**, *5*, 117–123.
- (35) Zhou, X.-F.; Oganov, A. R.; Wang, Z.; Popov, I. A.; Boldyrev, A. I.; Wang, H.-T. Two-dimensional magnetic boron. *Phys. Rev. B: Condens. Matter Mater. Phys.* **2016**, *93*, 085406.
- (36) Ivanov, A. S.; Miller, E.; Boldyrev, A. I.; Kameoka, Y.; Sato, T.; Tanaka, K. Pseudo Jahn-Teller Origin of Buckling Distortions in Two-Dimensional Triazine-Based Graphitic Carbon Nitride (g-C₃N₄) Sheets. *J. Phys. Chem. C* **2015**, *119*, 12008–12015.
- (37) Tkachenko, N. V.; Steglenko, D.; Fedik, N.; Boldyrev, N. M.; Minyaev, R. M.; Minkin, V. I.; Boldyrev, A. I. Superoctahedral two-dimensional metallic boron with peculiar magnetic properties. *Phys. Chem. Chem. Phys.* **2019**, *21*, 19764–19771.
- (38) Jena, P.; Sun, Q. Super Atomic Clusters: Design Rules and Potential for Building Blocks of Materials. *Chem. Rev.* **2018**, *118*, 5755–5870.
- (39) Galeev, T. R.; Dunnington, B. D.; Schmidt, J. R.; Boldyrev, A. I. Solid state adaptive natural density partitioning: a tool for deciphering multi-center bonding in periodic systems. *Phys. Chem. Chem. Phys.* **2013**, *15*, 5022–9.
- (40) Tang, W.; Sanville, E.; Henkelman, G. A grid-based Bader analysis algorithm without lattice bias. *J. Phys.: Condens. Matter* **2009**, *21*, 084204.
- (41) Yi, S.; Wang, C.; Jeon, H.; Cho, J.-H. Stabilization mechanism of clathrate H cages in a room-temperature superconductor LaH₁₀. *arXiv:2007.01531v1* 2020.
- (42) Evans, R. F.; Fan, W. J.; Chureemart, P.; Ostler, T. A.; Ellis, M. O.; Chantrell, R. W. Atomistic spin model simulations of magnetic nanomaterials. *J. Phys.: Condens. Matter* **2014**, *26*, 103202.
- (43) Peng, F.; Sun, Y.; Pickard, C. J.; Needs, R. J.; Wu, Q.; Ma, Y. Hydrogen Clathrate Structures in Rare Earth Hydrides at High Pressures: Possible Route to Room-Temperature Superconductivity. *Phys. Rev. Lett.* **2017**, *119*, 107001.
- (44) Semenok, D. V.; Kruglov, I. A.; Savkin, I. A.; Kvashnin, A. G.; Oganov, A. R. On Distribution of Superconductivity in Metal Hydrides. *Curr. Opin. Solid State Mater. Sci.* **2020**, *24*, 100808.